FISEVIER

Contents lists available at ScienceDirect

Advanced Powder Technology

journal homepage: www.elsevier.com/locate/apt



Rapid Communication

Data-driven parameter optimization for the synthesis of high-quality zeolitic imidazolate frameworks via a microdroplet route



Xiang He¹, Jianping Chen, Shane Albin, Zan Zhu, Wei-Ning Wang*

Department of Mechanical and Nuclear Engineering, Virginia Commonwealth University, Richmond, VA 23219, United States

ARTICLE INFO

Article history:
Received 4 August 2020
Received in revised form 14 November 2020
Accepted 17 November 2020
Available online 3 December 2020

Keywords: MOFs ZIFs Aerosol Genetic algorithm Multidimensional scaling

ABSTRACT

As an emerging strategy for the synthesis of metal-organic frameworks (MOFs), a microdroplet-based spray method holds merits of improved heat and mass transfer rates, which allows the formation of MOF crystals in a much faster manner. To optimize the spray route for the MOF synthesis, further exploration is needed to understand the dominant variables controlling the quality of the products. With a series of experiments and advanced computational analysis, we present here general guidance for the synthesis of representative zeolitic imidazolate frameworks (i.e., ZIF-8 and ZIF-67) using the spray route. © 2021 The Society of Powder Technology Japan. Published by Elsevier B.V. and The Society of Powder Technology Japan. All rights reserved.

1. Introduction

Metal-organic frameworks (MOFs) are a family of highly porous crystalline materials [1], which have great potentials in many applications, including but not limited to gas adsorption and separation, energy storage, and chemical sensing [2-5]. MOFs, as indicated by their names, are assembled through the coordination between metal nodes and organic ligands. Due to the intrinsic complexity of the three-dimensional (3D) crystalline structures, the synthesis of MOFs using the traditional solvothermal or hydrothermal methods typically requires long reaction time (e.g., from hours to days), mainly limited by the slow heat and mass transfer in these methods [6,7]. Recently, a microdroplet-based spray method (or the so-called aerosol route) has demonstrated to be an effective approach to synthesize MOFs in a much faster manner (i.e., within several seconds) [8-11]. In this method, the bulk precursor solution is atomized into microdroplets, which serve as microreactors for the formation of MOF crystals under both atmospheric [8–10] and low-pressure conditions [11]. Because of the small dimensions of the microdroplets, the heat

Abbreviations: BET, Brunauer-Emmett-Teller; ED, Euclidean distance; GA, genetic algorithm; HBD, hydrogen bond donation; MDS, multidimensional scaling; MOF, metal-organic frameworks; ZIF, zeolitic imidazolate frameworks.

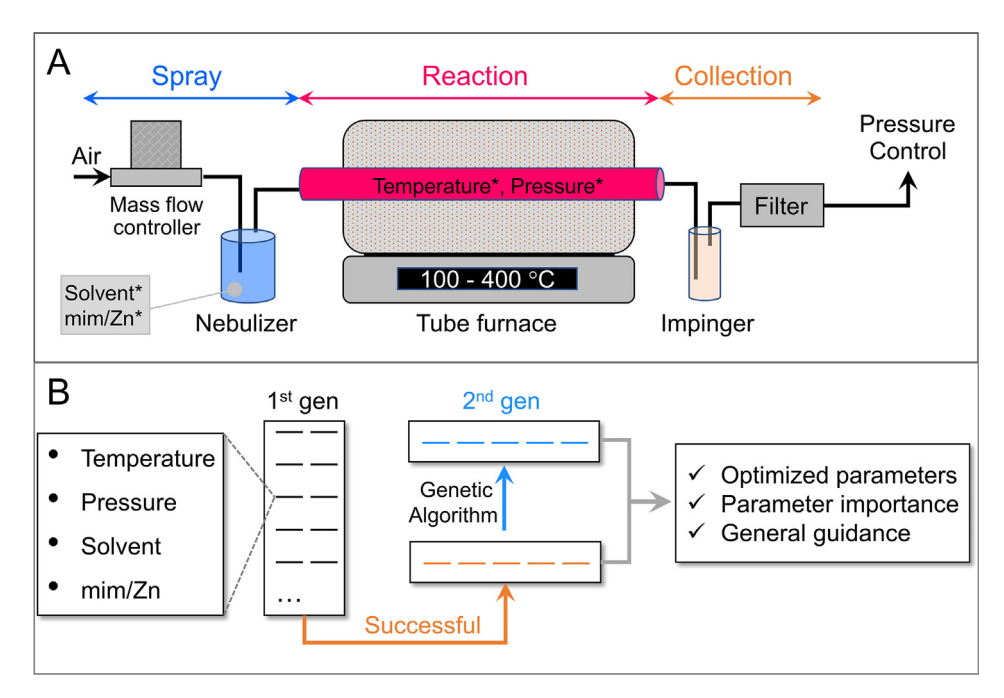
and mass transfer rates can be significantly enhanced, which subsequently contribute to the fastened nucleation and crystallization processes. In addition, the spray route is a continuous process which can also be easily scaled up for mass production of MOF particles [12,13]. Last but not least, the spray method has demonstrated to be capable of synthesizing mixed-component MOFs, designing MOF-based composites, and post-synthetic modification of MOFs, making it a versatile approach to rationally design novel MOF-based functional materials on demand [8-10,14,15]. It should be noted that the application of the microdroplet approach for the MOFs synthesis is still in its early stage, and more efforts are necessary for further understanding of the formation mechanism and dominating parameters. Targeting at this objective, we present here the exploration of dominating parameters for the synthesis of a representative MOF (i.e., ZIF-8 [16]) using the spray route with the aid of advanced computational methodologies, including multidimensional scaling (MDS), MaxMin algorithm, Euclidean distance (ED), genetic algorithm (GA), and univariate feature selection (i.e., F-test). An illustration of the spray system is shown in Scheme 1A, which consists of several components, including the spray section (e.g., the flow and pressure controllers, and a Collison Nebulizer), the reaction section (i.e., the tube furnace), and the product collection section (e.g., impinger and filter). The synthesis procedure is detailed in S1.

In a typical microdroplet-based spray process, there are four major parameters that are important for determining the properties of MOF products (e.g., particle size, crystallinity, and porosity), including the furnace temperature, the operating pressure, the solvent compositions (i.e., DI water/methanol (termed DI/MeOH

^{*} Corresponding author.

E-mail address: wnwang@vcu.edu (W.-N. Wang).

¹ Present addresses: Chemical Sciences and Engineering Division, Argonne National Laboratory, Lemont, IL 60439, United States.



Scheme 1. (A) Set-up of the spray system (* indicates synthesis parameters). (B) Logical flow of current study.

hereafter)), and organic linker/metal ion ratio (i.e., 2methylimidazole/Zn²⁺ (termed mim/Zn hereafter)) (Scheme 1A). As shown in Scheme 1B, by combing varying parameters together, we would have massive sets of experimental parameters for the synthesis of MOFs. To figure out the importance of the parameters and obtain general guidance with the least amount of trial and error, MaxMin algorithm and pairwise ED were firstly used to map out the most diverse 100 synthesis parameters using a web tool developed by Moosavi et al. [17] In brief, a parameter set was randomly selected from the pool of the normalized parameters to initiate the procedure. Then, the following sets were identified from the parameter pool by using MaxMin algorithm. Such a procedure continued until the first 100 parameter sets were determined. The synthesis parameters are detailed in Table S2, where each experimental set is indexed and the indexed numbers (i.e., #1, #2, #3...) will be used to indicate the corresponding assynthesized samples. Then, the synthesis of ZIF-8 was firstly carried out one by one using the first 21 parameter sets, which represent the most diverse parameter sets of all. Characterizations of the samples were conducted to pick out the successful ones (i.e., the ones exhibiting ZIF-8 crystalline structure). Five successful sample parameters were identified and then used as the first generation of datasets to reproduce the second generation of experimental parameter sets using GA (Scheme 1B), involving migration, crossover, and mutation operations. The objective of using GA here is to optimize the parameter set based on the first generation ones, which is similar to the natural evolution [17]. The optimization process was completed and terminated when the ZIF-8 product achieved a Brunauer-Emmett-Teller (BET) surface area comparable with the highest value reported in the literature. With the information obtained from all successful samples, the importance of each parameter was derived using the F-test, and general guidance for the synthesis of MOFs using the spray method was provided for future reference (Scheme 1B).

2. Results and discussion

In particular, MDS was applied to visualize the similarities among 100 parameters in the Euclidean space (Fig. 1A), where each

dot represents one synthesis parameter set. In principle, the distance between every two dots can be used to indicate the similarity level between these two parameter-sets. In other words, two dots (i.e., two parameter sets) having a shorter distance compared to others are similar to each other and vice versa. Notably, all the outermost (edge) nodes in the MDS plot, representing the most diverse dots, are covered by the first 21 experimental sets (i.e., orange dots in Fig. 1A), demonstrating that these 21 experimental sets have the most diversity within the defined chemical space. Therefore, we initially carried out the synthesis of ZIF-8 with the first 21 parameter sets. After synthesis, the samples were firstly characterized by powder X-ray diffraction (PXRD) measurements. Complete PXRD results are shown in Fig. S1, where various patterns indicate different degrees of crystallization. Among these 21 samples, only five samples (referred by blue indices in Fig. 1A) exhibit desired PXRD patterns, which are shown in Fig. 1B. The poor crystallization of the other samples is correlated to two reasons: (1) incomplete coordination (See Fig. S2) and (2) degradation of organic components at high temperature (i.e., 400 °C). The scanning electron microscopy (SEM) images of several typical samples are shown in Figs. S3-S5.

Despite their perfect PXRD patterns, these five successful samples exhibit minor differences regarding surface functional groups (Fig. 1C). In particular, there are two major groups of functional groups for ZIF-8 crystals. Specifically, the vibration band at 420 cm⁻¹ corresponds to Zn-N bonds, demonstrating the successful coordination of Zn ions and the ligand (i.e., mim). The peaks in the range of 600–1350 cm⁻¹ and 1350–1500 cm⁻¹ can be assigned to bending and stretching modes of imidazole units, respectively [18]. Marginal differences are observed among these five samples at 742 cm⁻¹, where the strongest peak of mim locates. This marginal variation suggests the existence of unreacted or partially reacted mim in the products, which could lead to different surface areas and porosities. To demonstrate this, N2 sorption at 77 K was performed to analyze the surface areas and the porosity properties of these samples after degassing at 150 °C under vacuum for 10 hrs. As shown in Fig. 1D, these five samples differ from each other in terms of both nitrogen sorption patterns and nitrogen uptake. Notably, every sample exhibits a rapid rise in the low relative

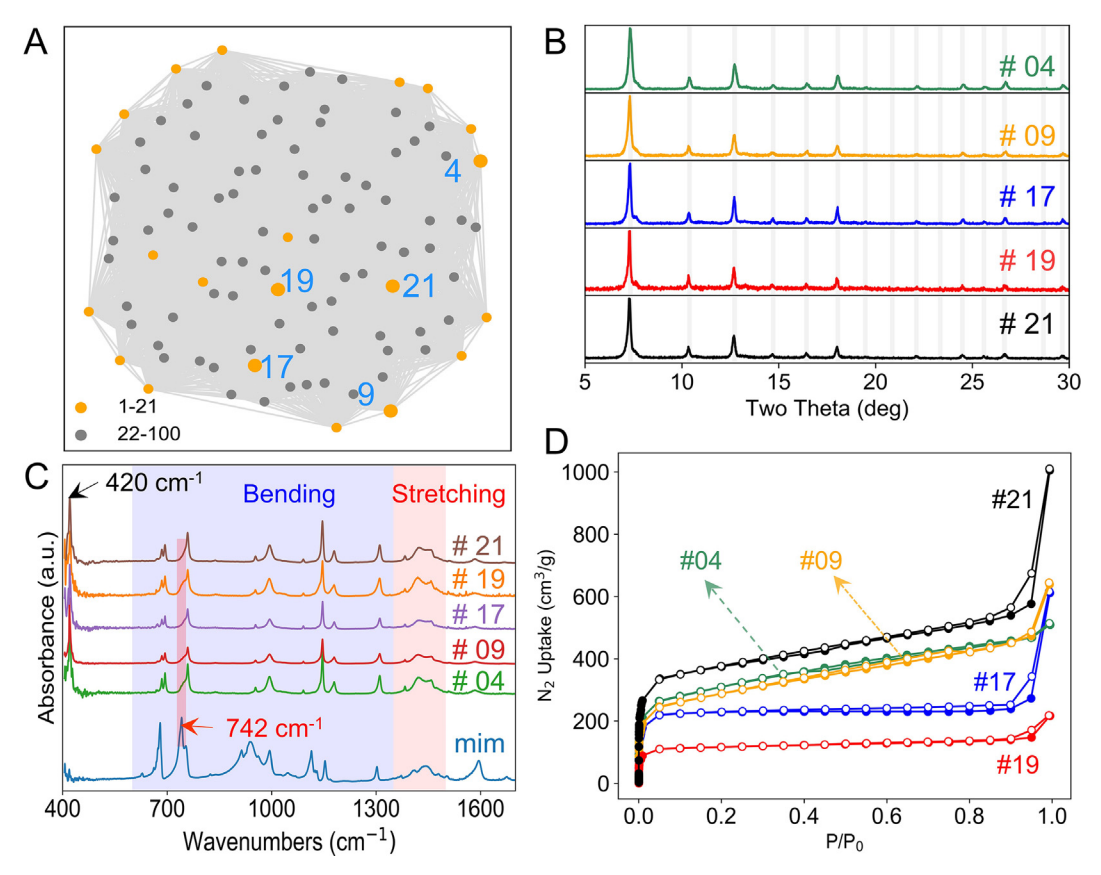


Fig. 1. (A) MDS plot of the most distinct 100 experimental parameter sets; (B) PXRD patterns, (C) FT-IR spectra, and (D) N₂ sorption (77 K) isotherms of the successfully synthesized ZIF-8 samples.

pressure region, suggesting the dominance of the microporous structures in the as-prepared samples. The lowest N₂ sorption uptake is observed with sample #19, which exhibits the smallest BET surface area of 472 m^2/g . In the first generation, the largest BET surface area is observed with the sample #21 (1442 m^2/g). Compared to that of sample #19, the sample #21 shows a rising N₂ uptake instead of a plateau in the middle relative pressure region and a hysteresis loop in the high relative pressure region, suggesting the existence of mesoporous structures in sample #21. To quantify the size distributions of the pores, non-local density functional theory (NLDFT) was applied (N2-carbon, 77 K, slitpore model) and results are shown in Fig. S6. As expected, all these five samples are dominated by micropores (i.e., 10.8 Å), which can be ascribed to the typical cage size of the ZIF-8 structure [19,20]. Consistent with the sorption isotherms, mesopores (i.e., 27.7-29.1 Å) are observed with several samples, such as #4, #9, and #21, which might be related to interparticle voids [21].

In order to get better ZIF-8 samples with higher BET surface areas, it is necessary to fine tune and optimize the synthesis parameters. To achieve that, GA was applied here to these five successful samples to derive a new generation of synthesis parameters. Specifically, GA is an optimization procedure inspired by natural evolution, which can select the best genes (i.e., experimental variables) from the parent experimental sets in the first generation, and reproduce optimized generation of experimental parameters (i.e., offspring) via migration, crossover, and mutation operations. This procedure is described in S4. The second generation of the synthesis parameters is defined as #101-#105 (Table S3).

Combining the new synthesis parameters with the original synthesis parameters, a new MDS plot is generated and shown in Fig. 2A. As expected, the new generation of the synthesis

parameters locates within the range of the previous five successful parameters, indicating the similarity among these samples. As a result, all the samples in the new generation exhibit good crystallinity with all the PXRD patterns matching with the simulated one (Fig. S7A). To unravel the evolution of the crystalline structures over the two generations, the Scherrer equation was used to calculate the crystallite sizes based on the full width at half maximum (FWHM) of the three strongest PXRD peaks (i.e., (011), (112), and (222)). As illustrated in Fig. 2B, the samples show minor differences in crystallite sizes over the two generations of optimization, which is reasonable as the optimization was proceeded using the BET surface area as the target. Notably, the crystallite size of # 21 (i.e., 53 nm) is much smaller than the particle size (i.e., 162 nm, the mean diameter derived from the SEM image (Fig. S5), suggesting that the as-obtained samples are polycrystalline products. The FT-IR spectra of the samples are obtained as in Fig. S7B, where all the samples exhibit similar vibrational bands with only marginal differences at the wavenumber of 742 cm⁻¹, suggesting the variations in the product qualities. Then, N2 sorption measurements were carried out to analyze the surface areas and pore size distributions of the samples. The isotherms of the N₂ sorption are shown in Fig. S8A. Like those in the first generation, the isotherms of all these five samples show steep rises in the low relative pressure region, demonstrating that the porous structures of these samples are still dominated by micropores. The corresponding pore size distributions are shown in Fig. S8B, which exhibits consistent results. To achieve a big picture of how the porous structures evolved during the exploration process, the corresponding results are summarized and presented in Fig. 2C. In the first generation, the BET surface areas range from 472 to 1442 m²/g. After the genetic algorithm, the BET surface areas are improved to the range of 608 to 1748 m²/g, indicating the effectiveness of

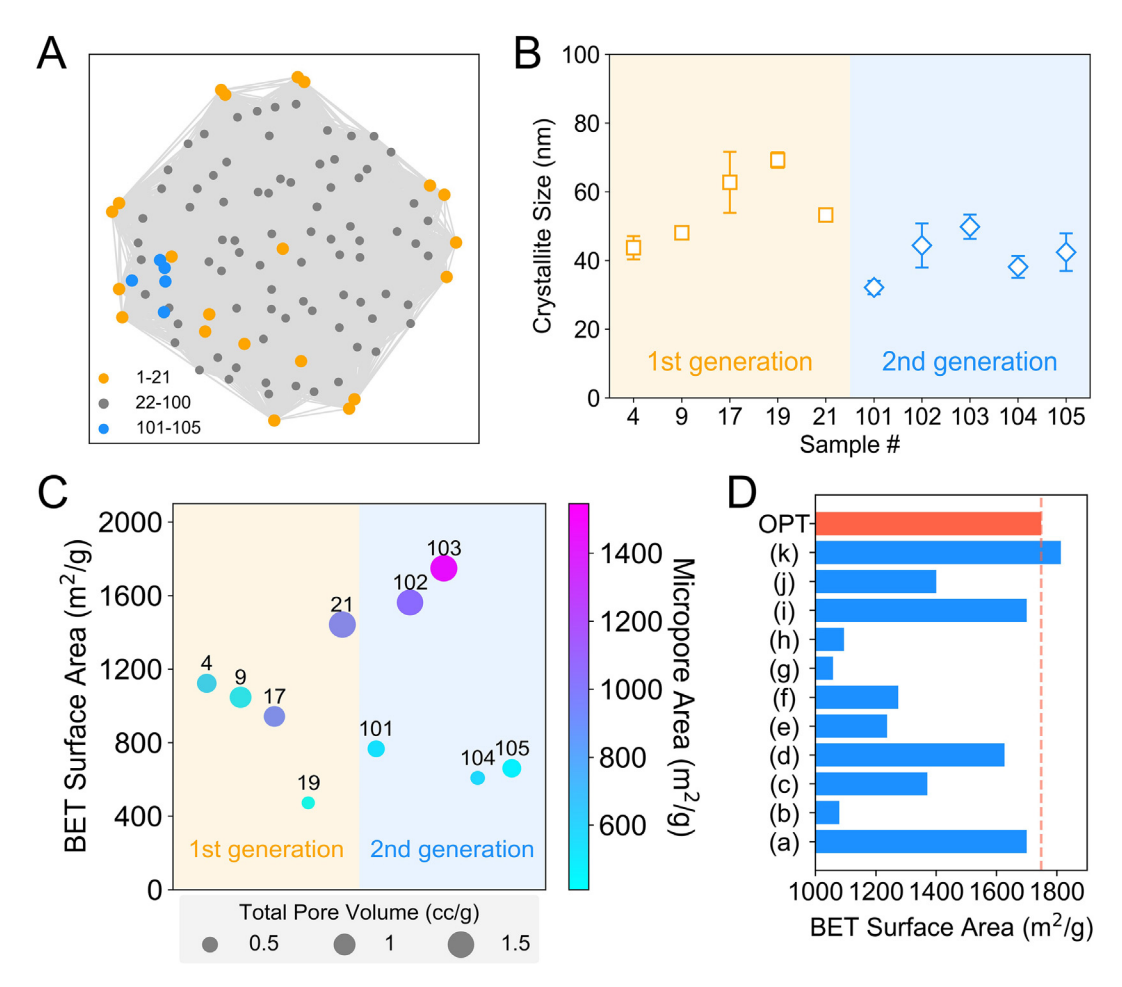


Fig. 2. (A) MDS plot of the experimental sets; (B) Crystallite sizes; (C) Textural properties; (D) Comparison of surface area of the optimum (OPT) sample (#103) with reported ones (i.e., (a-j) [21–29] and (k): Sigma-Aldrich product). Note: #101-#105 are 2nd-generation samples reproduced from successful sets in 1st generation (i.e., #4, #9, #17, #19, #21) via GA.

using GA to improve the quality of the products. Along with BET surface areas, samples also exhibit variations in total pore volumes and micropore areas. Overall, the values of the total pore volumes and micropore areas show a positive relationship with the BET surface areas (Fig. S9). The highest BET surface area is observed for sample #103 with a value of 1748 m²/g, which is among the highest reported values (Fig. 2D).

In order to understand the parameter-property relationship and derive general guidance for the synthesis of MOFs using the spray method, F-test was applied here to estimate the dependence of the product quality against each parameter. Specifically, all 21 samples in the first generation and the five samples in the second generation were classified into two categories (i.e., successful and unsuccessful) based on their PXRD patterns. Then, F-test was used to find the parameter that mostly affects the successful formation of the crystals. As shown in Fig. 3A, the reaction temperature exhibits the highest F-value, suggesting the dominating role of the reaction temperature in successful/unsuccessful formation of MOF crystals in microdroplets. This is reasonable as the nucleation and crystal growth are mainly driven by the evaporation of microdroplets, which has a great dependence on the reaction temperature [11]. Following temperature, the ratios of DI/MeOH and mim/Zn also play an important role. The effects of DI/MeOH ratio on the crystal formation might originate from the variance in the hydrogen bond donation (HBD) ability of the solvents [30]. In particular, the formation of ZIF-8 crystals occurs through the assembly of Zn²⁺ and mim, where Zn²⁺ ions coordinate with the N atoms in mim molecules. This process leads to the polarization of protons in mim and can be greatly influenced by the HBD capacity of solvents. Since water and MeOH have different HBD values (i.e., water: 1.17, MeOH: 0.98) [30], it is no surprise that the changing ratios of DI/MeOH would greatly affect the formation of ZIF-8. On the other hand, the mim/Zn ratio mainly affects the ZIF-8 formation via modulating the reaction kinetics and the existing forms of mim. Specifically, excessive mim molecules could exist in both deprotonated form as linkers and the neutral form as stabilizing agents [31], which should play an important role in the subsequent crystal formation process. In comparison to the above-mentioned parameters, the operating pressure shows a lower F-value, indicating its minor importance in ZIF-8 synthesis. From these F-values, it is derived that, for future exploration of MOF synthesis using the spray method, it is more efficient to screen the effects of temperature first, then the effects of solvent and metal/linker ratios. It should be noted that, the operating pressure does have effects on the properties of the MOF products (e.g., crystalline structure and morphology) [11]. However, it may not be the major parameter to adjust in order to achieve the successful synthesis of MOFs. After the successful synthesis of MOFs, the next objective is to further improve the textural properties of the products by fine tuning the experimental parameters. Therefore, it is important to know the dependency of the quality of MOFs (i.e., surface area) against each synthesis parameter. In terms of this, F-test for regression was carried out to analyze the data of the successful 10 samples from the two generations. Specifically, the BET surface areas were

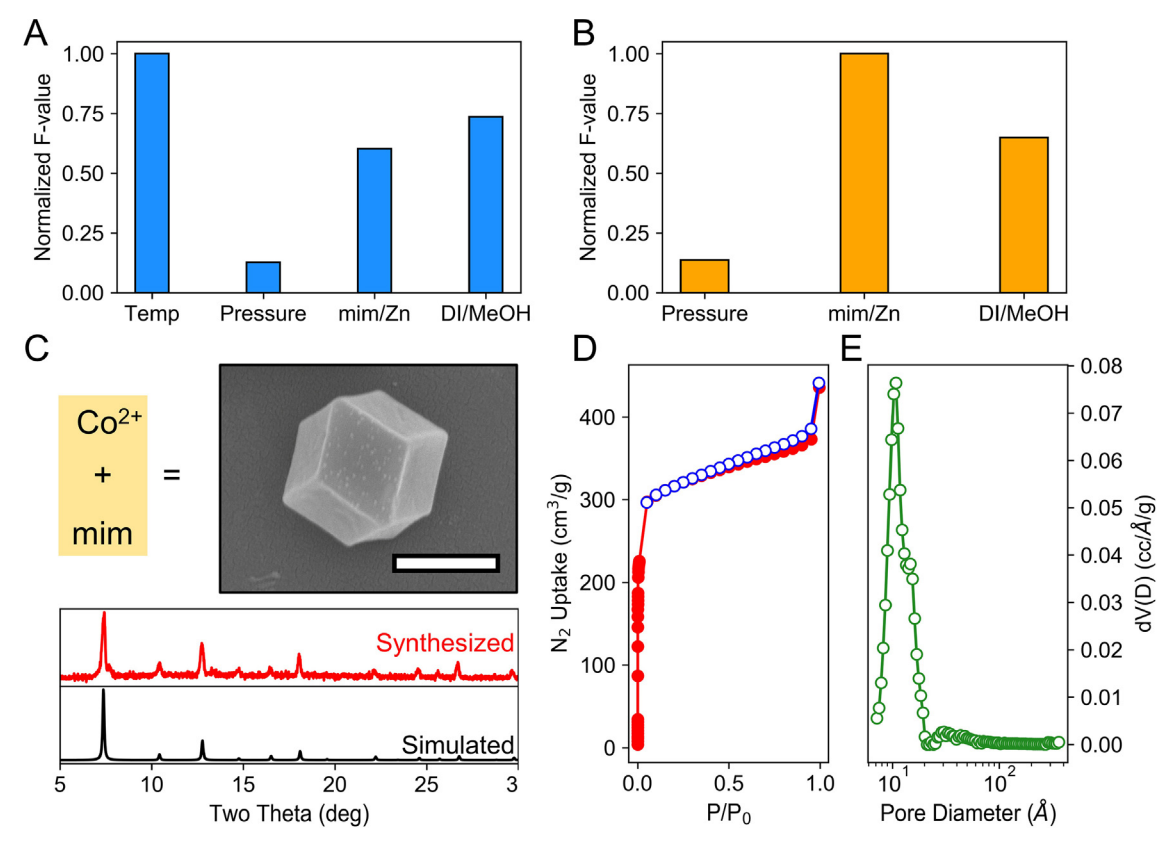


Fig. 3. (A) Normalized F-values of each parameter to get successfully synthesized ZIF-8; (B) Normalized F-values of each parameter to synthesize ZIF-8 with higher BET surface area; (C) SEM image and PXRD pattern (scale bar: 500 nm), (D) N₂ sorption isotherm, and (E) pore size distribution (DFT method) of as-synthesized ZIF-67.

used as the target variable. The correlation between each parameter and the BET surface area was analyzed with F-test for regression. It should be noted that the temperature parameter was not taken into consideration as all these 10 samples were synthesized at 100 °C. The corresponding F-values are summarized in Fig. 3B. In comparison, mim/Zn ratio shows the highest F-value followed by DI/MeOH then the operating pressure, which suggests the importance sequence of the parameters as follows: mim/Zn ratio > DI/MeOH > pressure.

To verify the universality of the above findings, the optimized parameter set was applied to synthesize other ZIFs. As an example, ZIF-67 was successfully synthesized by using the same synthesis parameters as those of sample #103, except that Zn²⁺ was replaced with Co²⁺ (Fig. 3C). The as-synthesized ZIF-67 exhibits perfect rhombic dodecahedron shape (Fig. 3C and Fig. S10), suggesting that the sample is fully crystallized. The PXRD pattern of the as-prepared ZIF-67 is shown in Fig. 3C, which agrees well with the simulated pattern, further demonstrating the good crystalline structure and suggesting that the as-discovered parameters can be used to synthesize the ZIFs that are isostructural to ZIF-8. The N₂ sorption isotherm of ZIF-67 is shown in Fig. 3D, from which the BET surface area is derived to be 1273 m²/g. This value is also comparable to those reported in prior studies [32,33]. The pore size distribution of ZIF-67 was calculated using NLDFT method, and the result is shown in Fig. 3E. As expected, the pores inside ZIF-67 are dominated by micropores, with characteristic pore diameters of 10.8 Å, which is the same as that of the ZIF-8 samples.

3. Conclusions

In summary, general guidance is presented here for the MOFs synthesis using the spray process with a series of advanced techniques (e.g., ED, GA, and F-test). The results indicate that temperature plays the most significant role in the formation of MOF crystals during the spray process. Besides, the solvent and precursors could also be deliberately adjusted to achieve optimal products.

Funding sources

This work is funded by the National Science Foundation (CMMI-1727553).

Declaration of Competing Interest

The authors declare that they have no known competing financial interests or personal relationships that could have appeared to influence the work reported in this paper.

Acknowledgment

National Science Foundation (CMMI-1727553) is greatly acknowledged for the funding.

Appendix A. Supplementary data

Supplementary data to this article can be found online at https://doi.org/10.1016/j.apt.2020.11.018.

References

- [1] O.M. Yaghi, M. O'Keeffe, N.W. Ockwig, H.K. Chae, M. Eddaoudi, J. Kim, Reticular synthesis and the design of new materials, Nature 423 (2003) 705–714.
- [2] L.J. Murray, M. Dinca, J.R. Long, Hydrogen storage in metal-organic frameworks, Chem. Soc. Rev. 38 (2009) 1294–1314.
- [3] S. Yuan, L. Feng, K. Wang, J. Pang, M. Bosch, C. Lollar, Y. Sun, J. Qin, X. Yang, P. Zhang, Q. Wang, L. Zou, Y. Zhang, L. Zhang, Y. Fang, J. Li, H.C. Zhou, Stable metal-organic frameworks: design, synthesis, and applications, Adv. Mater. 30 (2018) 1704303.
- [4] J. Yu, L.-H. Xie, J.-R. Li, Y. Ma, J.M. Seminario, P.B. Balbuena, CO2 capture and separations using MOFs: computational and experimental studies, Chem. Rev. 117 (2017) 9674–9754.
- [5] L.E. Kreno, K. Leong, O.K. Farha, M. Allendorf, R.P. Van Duyne, J.T. Hupp, Metalorganic framework materials as chemical sensors, Chem. Rev. 112 (2012) 1105–1125.
- [6] N. Stock, S. Biswas, Synthesis of metal-organic frameworks (MOFs): routes to various MOF topologies, morphologies, and composites, Chem. Rev. 112 (2012) 033_060
- [7] S.R. Venna, J.B. Jasinski, M.A. Carreon, Structural evolution of zeolitic imidazolate framework-8, J. Am. Chem. Soc. 132 (2010) 18030–18033.
- [8] A. Carné-Sánchez, I. Imaz, M. Cano-Sarabia, D. Maspoch, A spray-drying strategy for synthesis of nanoscale metal-organic frameworks and their assembly into hollow superstructures, Nat. Chem. 5 (2013) 203–211.
- [9] X. He, Z.R. Gan, S. Fisenko, D.W. Wang, H.M. El-Kaderi, W.N. Wang, Rapid formation of metal-organic frameworks (MOFs) based nanocomposites in microdroplets and their applications for CO2 photoreduction, Acs Appl Mater Inter 9 (2017) 9688–9698.
- [10] L. Garzón-Tovar, S. Rodríguez-Hermida, I. Imaz, D. Maspoch, Spray drying for making covalent chemistry: postsynthetic modification of metal-organic frameworks, J. Am. Chem. Soc. 139 (2017) 897–903.
- [11] X. He, W.-N. Wang, Pressure-regulated synthesis of Cu(TPA) (DMF) in microdroplets for selective CO2 adsorption, Dalton T 48 (2019) 1006–1016.
- [12] K. Okuyama, I.W. Lenggoro, Preparation of nanoparticles via spray route, Chem. Eng. Sci. 58 (2003) 537–547.
- [13] W.N. Wang, I.W. Lenggoro, K. Okuyama, Preparation of nanoparticles by spray routes, in: H.S. Nalwa (Ed.), Encyclopedia of Nanoscience and Nanotechnology, American Scientific Publishers, 2011, pp. 435–458.
 [14] X. He, D.-R. Chen, W.-N. Wang, Bimetallic metal-organic frameworks (MOFs)
- [14] X. He, D.-R. Chen, W.-N. Wang, Bimetallic metal-organic frameworks (MOFs) synthesized using the spray method for tunable CO2 adsorption, Chem. Eng. J. 382 (2020) 122825.
- [15] X. He, W.-N. Wang, Synthesis of Cu-trimesic Acid/Cu-1,4-benzenedioic acid via microdroplets: role of component compositions, Cryst. Growth Des. 19 (2019) 1095–1102.
- [16] R. Banerjee, A. Phan, B. Wang, C. Knobler, H. Furukawa, M. O'Keeffe, O.M. Yaghi, High-throughput synthesis of zeolitic imidazolate frameworks and application to CO₂ capture, Science 319 (2008) 939–943.

- [17] S.M. Moosavi, A. Chidambaram, L. Talirz, M. Haranczyk, K.C. Stylianou, B. Smit, Capturing chemical intuition in synthesis of metal-organic frameworks, Nat. Commun. 10 (2019) 539.
- [18] X. He, C. Yang, D. Wang, S.E. Gilliland Iii, D.-R. Chen, W.-N. Wang, Facile synthesis of ZnO@ZIF core-shell nanofibers: crystal growth and gas adsorption, CrystEngComm 19 (2017) 2445–2450.
- [19] Q. Song, S.K. Nataraj, M.V. Roussenova, J.C. Tan, D.J. Hughes, W. Li, P. Bourgoin, M.A. Alam, A.K. Cheetham, S.A. Al-Muhtaseb, E. Sivaniah, Zeolitic imidazolate framework (ZIF-8) based polymer nanocomposite membranes for gas separation, Energy Environ. Sci. 5 (2012) 8359–8369.
- [20] M.J.C. Ordoñez, K.J. Balkus, J.P. Ferraris, I.H. Musselman, Molecular sieving realized with ZIF-8/Matrimid[®] mixed-matrix membranes, J. Memb. Sci. 361 (2010) 28–37.
- [21] A. Schejn, L. Balan, V. Falk, L. Aranda, G. Medjahdi, R. Schneider, Controlling ZIF-8 nano- and microcrystal formation and reactivity through zinc salt variations, CrystEngComm 16 (2014) 4493–4500.
- [22] Y. Pan, Y. Liu, G. Zeng, L. Zhao, Z. Lai, Rapid synthesis of zeolitic imidazolate framework-8 (ZIF-8) nanocrystals in an aqueous system, Chem. Commun. 47 (2011) 2071–2073.
- [23] Z. Yang, H. Li, J. Yang, S. Feng, X. Liu, J. Zhao, W. Qu, P. Li, Y. Feng, P.-H. Lee, K. Shih, Nanosized copper selenide functionalized zeolitic imidazolate framework-8 (CuSe/ZIF-8) for efficient immobilization of gas-phase elemental mercury, Adv. Funct. Mater. 29 (2019) 1807191.
- [24] J. Liu, R. Li, Y. Hu, T. Li, Z. Jia, Y. Wang, Y. Wang, X. Zhang, C. Fan, Harnessing Ag nanofilm as an electrons transfer mediator for enhanced visible light photocatalytic performance of Ag@AgCl/Ag nanofilm/ZIF-8 photocatalyst, Appl. Catal. B 202 (2017) 64–71.
- [25] J. Dai, X. Xiao, S. Duan, J. Liu, J. He, J. Lei, L. Wang, Synthesis of novel microporous nanocomposites of ZIF-8 on multiwalled carbon nanotubes for adsorptive removing benzoic acid from water, Chem. Eng. J. 331 (2018) 64–74.
- [26] M. Mohamedali, H. Ibrahim, A. Henni, Incorporation of acetate-based ionic liquids into a zeolitic imidazolate framework (ZIF-8) as efficient sorbents for carbon dioxide capture, Chem. Eng. J. 334 (2018) 817–828.
- [27] G. Liu, Y. Xu, Y. Han, J. Wu, J. Xu, H. Meng, X. Zhang, Immobilization of lysozyme proteins on a hierarchical zeolitic imidazolate framework (ZIF-8), Dalton T 46 (2017) 2114–2121.
- [28] A. Schejn, A. Aboulaich, L. Balan, V. Falk, J. Lalevée, G. Medjahdi, L. Aranda, K. Mozet, R. Schneider, Cu2+-doped zeolitic imidazolate frameworks (ZIF-8): efficient and stable catalysts for cycloadditions and condensation reactions, Catal. Sci. Technol. 5 (2015) 1829–1839.
- [29] X. Li, G. Liu, D. Xu, X. Hong, S.C. Edman Tsang, Confinement of subnanometric PdZn at a defect enriched ZnO/ZIF-8 interface for efficient and selective CO2 hydrogenation to methanol, J. Mater. Chem. A 7 (2019) 23878–23885.
- [30] E.L. Bustamante, J.L. Fernández, J.M. Zamaro, Influence of the solvent in the synthesis of zeolitic imidazolate framework-8 (ZIF-8) nanocrystals at room temperature, J Colloid Interf Sci 424 (2014) 37–43.
- [31] Y.-S. Li, F.-Y. Liang, H. Bux, A. Feldhoff, W.-S. Yang, J. Caro, Molecular sieve membrane: supported metal-organic framework with high hydrogen selectivity, Angew. Chem. Int. Ed. 49 (2010) 548–551.
- [32] Q. Yang, S. Ren, Q. Zhao, R. Lu, C. Hang, Z. Chen, H. Zheng, Selective separation of methyl orange from water using magnetic ZIF-67 composites, Chem. Eng. J. 333 (2018) 49–57.
- [33] Q. Shi, Z. Chen, Z. Song, J. Li, J. Dong, Synthesis of ZIF-8 and ZIF-67 by steamassisted conversion and an investigation of their tribological behaviors, Angew. Chem. Int. Ed. 50 (2011) 672–675.

Data-driven parameter optimization for the synthesis of high-quality zeolitic imidazolate frameworks via a microdroplet route

Xiang He, Jianping Chen, Shane Albin, Zan Zhu and Wei-Ning Wang*

Department of Mechanical and Nuclear Engineering, Virginia Commonwealth University, Richmond, Virginia 23219, USA.

Corresponding Author

*Wei-Ning Wang: Tel: 1-(804) 827-4306; Fax: 1-(804) 827-7030; Email: wnwang@ycu.edu

S1. CHEMICALS AND SYNTHESIS PARAMETERS

S1.1 Chemicals: $Zn(NO_3)_2 \cdot 6H_2O \ (\ge 99.0\%)$, 2-methylimidazole (mim, 99%), and $Co(NO_3)_2 \cdot 6H_2O \ (\ge 98.0\%)$ were purchased from Sigma-Aldrich, Acros Organics, and Fluka, respectively. All chemicals were used without further purification.

S1.2 Synthesis Parameters and Procedures

General Parameters and Procedures. For the aerosol synthesis set-up studied in this work, there are four major parameters that could be adjusted for the synthesis of ZIF-8, including temperature, pressure, mim/Zn ratio, and solvent conditions. Based on the current instrumental limitations, the range of each parameter that can be adjusted was determined as shown in **Table S1.1**. Typically, a precursor solution was prepared based on the experimental parameters and then loaded in the Collison Nebulizer¹ for aerosolization (**Scheme 1**). It should be mentioned that the precursor solution was kept under stirring before being aerosolized to avoid the precipitation. After the sequential spray, reaction, and collection processes, the products were collected and then washed with methanol through the centrifugation-redispersion cycle for three times. Finally, the products were dried in vacuum at 50 °C before further analysis.

Table S1.1. Variables for the aerosol synthesis and their corresponding ranges.

Variables	Range
Temperature (°C)	100 to 400
Pressure (-inHg)	22 to 0
mim/Zn (mol/mol)	1 to 15
DI/MeOH	0 to 1 (volume fraction of DI)

Note: (1) mim stands for 2-methylimidazole; Zn represents Zn(NO₃)₂·6H₂O; DI indicates deionized water; MeOH is short for methanol.

- (2) The concentration of Zn(NO₃)₂·6H₂O was fixed at 16.67 g/L.
- (3) DI/MeOH = 0 means only methanol was used as the solvent; DI/MeOH = 1 means only deionized water was used as the solvent.

Estimated Spray Time. Typically, a volume of 15 mL was used for the spray process, which was kept running until the precursor solution was consumed or unable to be aerosolized. Therefore, the spray time is controlled by how fast the precursor solution can be aerosolized and consumed, and it varies from each other under different synthesis conditions mainly because of the varying properties of solvent mixtures (e.g., the feasibility for aerosolization). To estimate the spray time, we sprayed the solvent mixtures under different synthesis conditions and measured the solvent consumption rate, from which we calculated the approximated time for the spray process. As shown in **Table S1.2**, if methanol is involved in the solvent mixtures, the spray time ranges from 0.19 h to 0.83 h. In general, the presence of water would slow down the spray process.

Table S1.2 Estimated time for the spray process.

Temperature (°C)	Pressure (-inHg)	DI (mL)	Methanol (mL)	Consumption Rate (mL/min)	Estimated Spray Time (h)
100	0	0	15	0.3	0.83
100	22	0	15	0.9	0.28
100	11	0	15	0.7	0.36
100	22	7.5	7.5	0.6	0.42
100	11	7.5	7.5	0.4	0.63
100	22	15	0	0.4	0.63
100	0	15	0	0.1	2.50
100	11	15	0	0.2	1.25
250	11	7.5	7.5	0.5	0.50
400	22	0	15	1.35	0.19
400	0	0	15	0.45	0.56
400	22	15	0	0.25	1.00

S1.3 Generation of the 100 Most Distinct Parameters for the Synthesis of ZIF-8

Firstly, each parameter was normalized based on their corresponding ranges. Then, the first parameter set was randomly selected. After that, the following parameter sets were determined through the MaxMin algorithm from parameter pool. A convenient web tool was developed by Moosavi *et al.*,² which can be easily applied to generate the diverse parameter sets as needed. Below in **Table S2**, we present the as-obtained the 100 most distinct parameter sets for the ZIF-8 synthesis.

Table S2. 100 most distinct parameter sets for the synthesis of ZIF-8.

Sample Numbers	Temperature (°C)	Pressure (-inHg)	mim/Zn (mol/mol)	DI/MeOH
1	400	0	15	1
2	100	22	15	1
3	100	0	1	1
4	100	0	15	0
5	400	22	1	1
6	400	22	15	0
7	400	0	1	0
8	100	22	1	1
9	100	22	15	0
10	100	0	1	0
11	100	0	15	1
12	250	11	8	0.5

13	400	22	1	0
14	400	22	15	1
15	400	0	1	1
16	400	0	15	0
17	100	22	8	0.5
18	100	11	1	0.5
19	100	11	8	0
20	100	11	8	1
21	100	11	15	0.5
22	100	0	8	0.5
23	250	22	1	0.5
24	250	22	8	0
25	250	22	8	1
26	250	22	15	0.5
27	250	11	1	0
28	250	11	1	1
29	250	11	15	0
30	250	11	15	1
31	250	0	1	0.5
32	250	0	8	0.5
33	250	0	8	1
34	250	0	15	0.5
35	400	22	8	0.5
36	400	11	1	0.5
37	400	11	8	0.3
38	400	11	8	1
39	400	11	15	0.5
40		0		
40	400 100	22	8 1	0.5
42				0.5
	100	22	8	0
43	100	22	8	1
44	100	22	15	0.5
45	100	11	1	0
46	100	11	1	1
47	100	11	8	0.5
48	100	11	15	0
49	100	11	15	1
50	100	0	1	0.5
51	100	0	8	0
52	100	0	8	1
53	100	0	15	0.5
54	175	16.5	4.5	0.25
55	175	16.5	4.5	0.75
56	175	16.5	11.5	0.25
57	175	16.5	11.5	0.75
58	175	5.5	4.5	0.25

59	175	5.5	4.5	0.75
60	175	5.5	11.5	0.25
61	175	5.5	11.5	0.75
62	250	22	1	0
63	250	22	1	1
64	250	22	8	0.5
65	250	22	15	0
66	250	22	15	1
67	250	11	1	0.5
68	250	11	8	0
69	250	11	8	1
70	250	11	15	0.5
71	250	0	1	0
72	250	0	1	1
73	250	0	8	0.5
74	250	0	15	0
75	250	0	15	1
76	325	16.5	4.5	0.25
77	325	16.5	4.5	0.75
78	325	16.5	11.5	0.25
79	325	16.5	11.5	0.75
80	325	5.5	4.5	0.25
81	325	5.5	4.5	0.75
82	325	5.5	11.5	0.25
83	325	5.5	11.5	0.75
84	400	22	1	0.5
85	400	22	8	0
86	400	22	8	1
87	400	22	15	0.5
88	400	11	1	0
89	400	11	1	1
90	400	11	8	0.5
91	400	11	15	0
92	400	11	15	1
93	400	0	1	0.5
94	400	0	8	0
95	400	0	8	1
96	400	0	15	0.5
97	100	22	4.5	0.25
98	100	22	4.5	0.75
99	100	22	11.5	0.25
100	100	22	11.5	0.75
-			="	- · · · ·

S2. CHARACTERIZATION METHODS

Powder X-ray diffraction (PXRD) patterns, textural porosities, scanning electron microscope (SEM) images, Fourier transform infrared (FT-IR) spectra of the samples were obtained by the PANalytical X-ray diffractometer (X'Pert PRO), Autosorb iQ, Hitachi SU-70, and Nicolet iS50 spectrometer, respectively.

S3. CHARACTERIZATIONS OF THE FIRST GENERATION OF SAMPLES

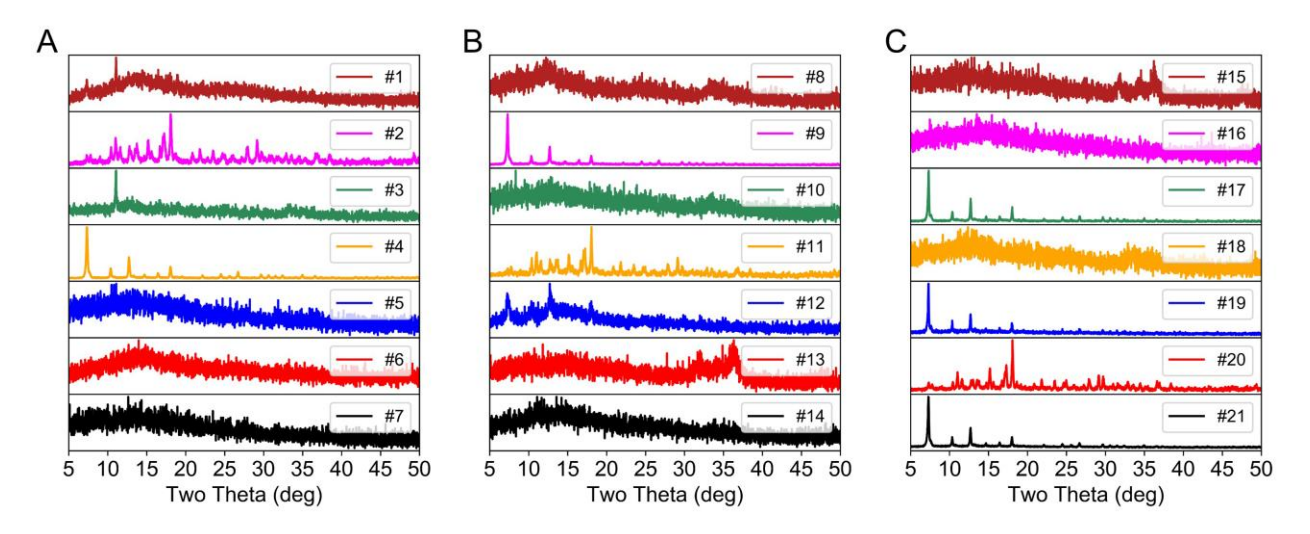


Figure S1. PXRD patterns of as-prepared samples. (A): #1 to #7; (B) #8 to #14; (C) #15 to #21.

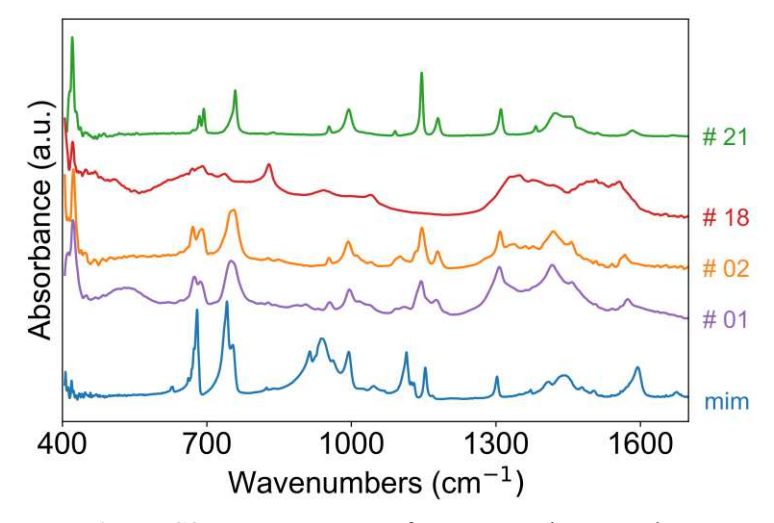


Figure S2. FT-IR spectra of representative samples.

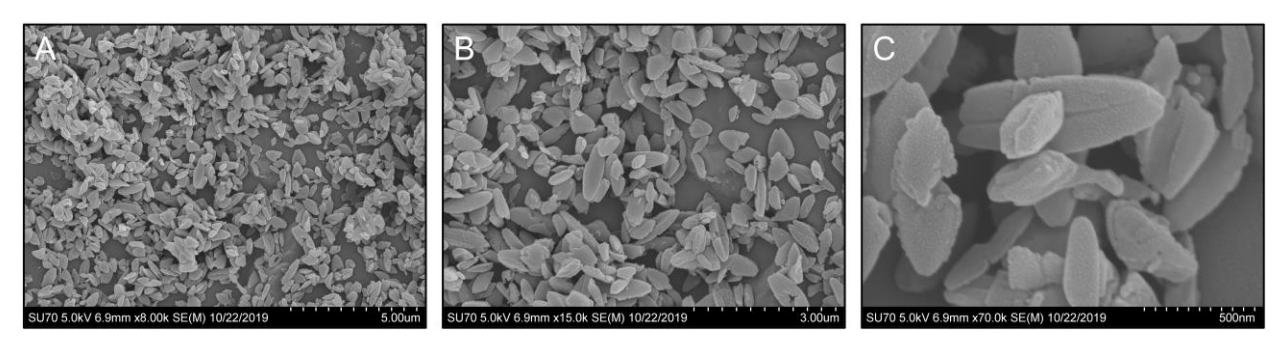


Figure S3. SEM images of **sample #2**. Magnifications: (A) ×8k; (B) ×15k; (C) ×70k.

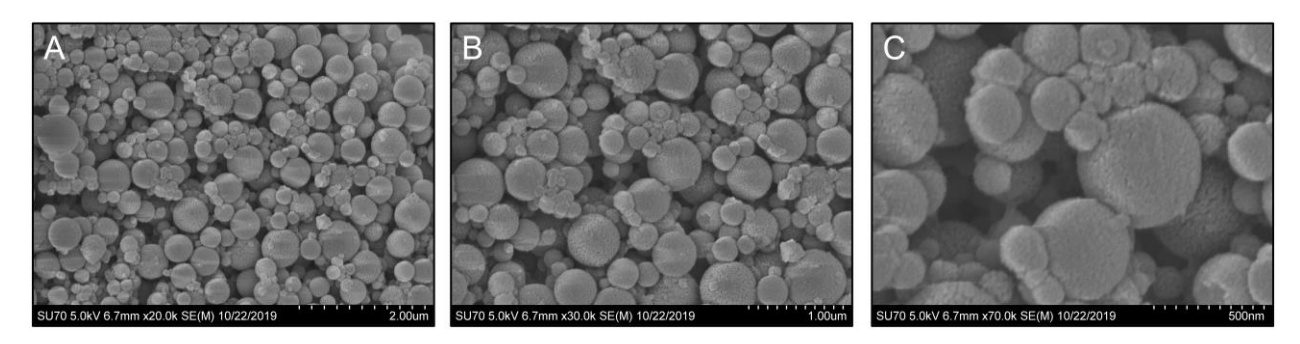


Figure S4. SEM images of **sample #6**. Magnifications: (A) ×20k; (B) ×30k; (C) ×70k.

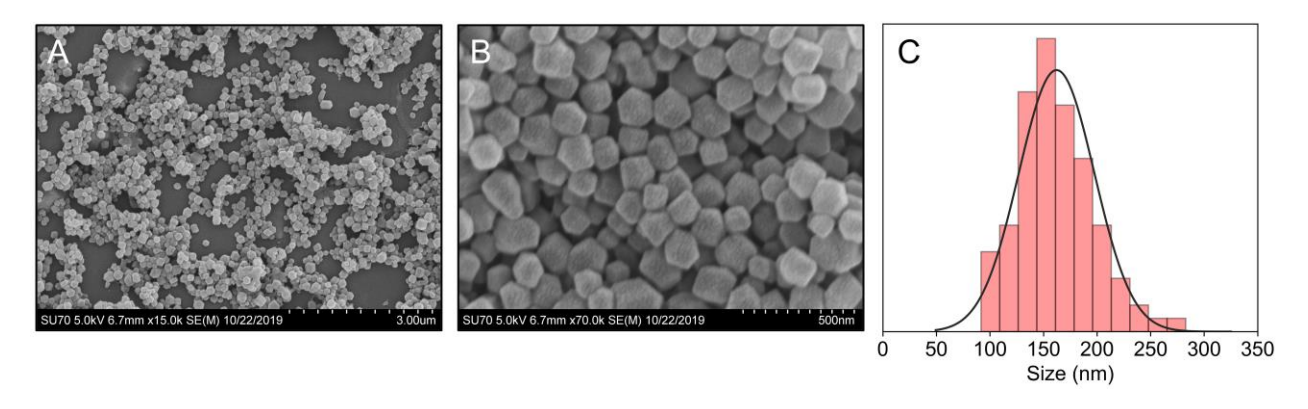


Figure S5. SEM images of **sample #21**. Magnifications: (A) ×15k; (B) ×70k. (C) Size distribution of sample #21.

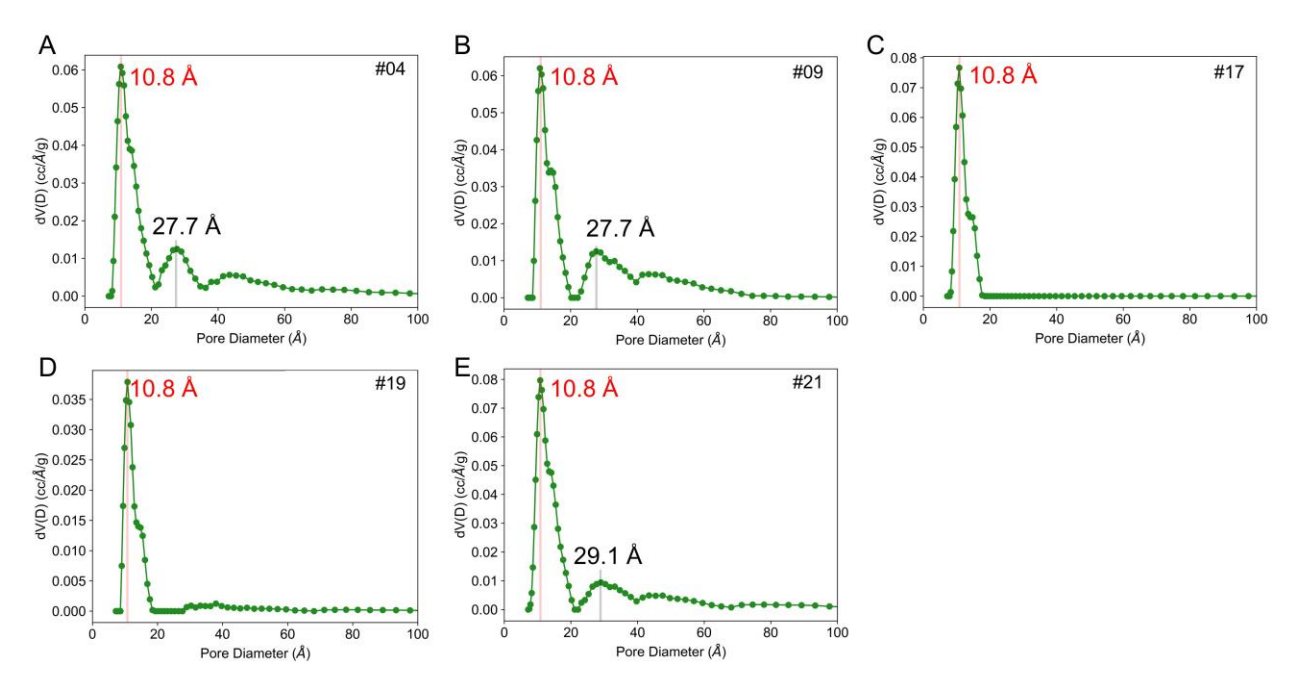


Figure S6. Pore size distributions of samples. (A) #4; (B) #9; (C) #17; (D) #19; (E) #21.

S4. SYNTHESIS PARAMETERS FOR THE SECOND GENERATION OF SAMPLES

To get higher surface area, the first five successful experimental sets (i.e., #4, #9, #17, #19, and #21) were used as the parent batch to derive the second batch of experimental sets by using genetic algorithm through a web tool developed by Moosavi *et al.*² In brief, a pair of experimental sets were randomly selected from the above five successful experimental sets and then subjected to migration, crossover, and mutation operations to reproduce new experimental sets as shown in **Table S3**.

Table S3. Synthesis parameters of the successful ZIF-8 samples. The production yield of the first generation is estimated based on **Table S1.2**, assuming all ingredients are converted and all products are collected.

Generations	Sample #	Temperature (°C)	Pressure (-inHg)	mim/Zn (mol/mol)	DI/MeOH	Yield (g/h)
	4	100	0	15	0	1.044
	9	100	22	15	0	3.133
First	17	100	22	8	0.5	2.089
	19	100	11	8	0	2.437
	21	100	11	15	0.5	1.393
	101	100	13	12.55	0	
Second	102	100	15	15	0.37	
	103	100	12	15	0.21	
	104	100	22	11.21	0.14	
	105	100	19	14.97	0.03	

S5. CHARACTERIZATIONS OF THE SECOND GENERATION OF SAMPLES

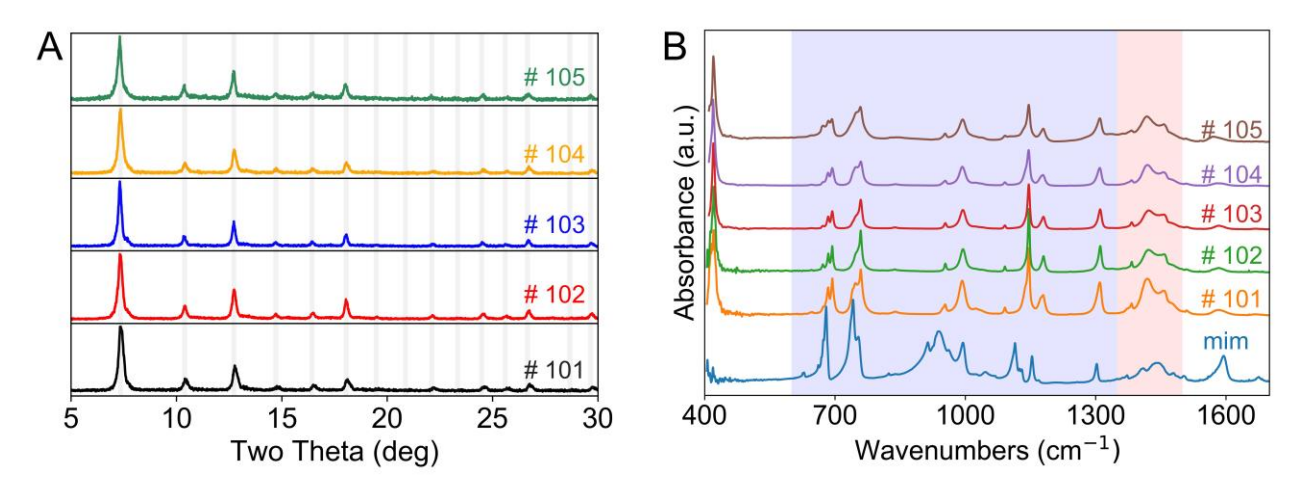


Figure S7. (A) PXRD patterns and (B) FT-IR spectra of samples #101 to #105.

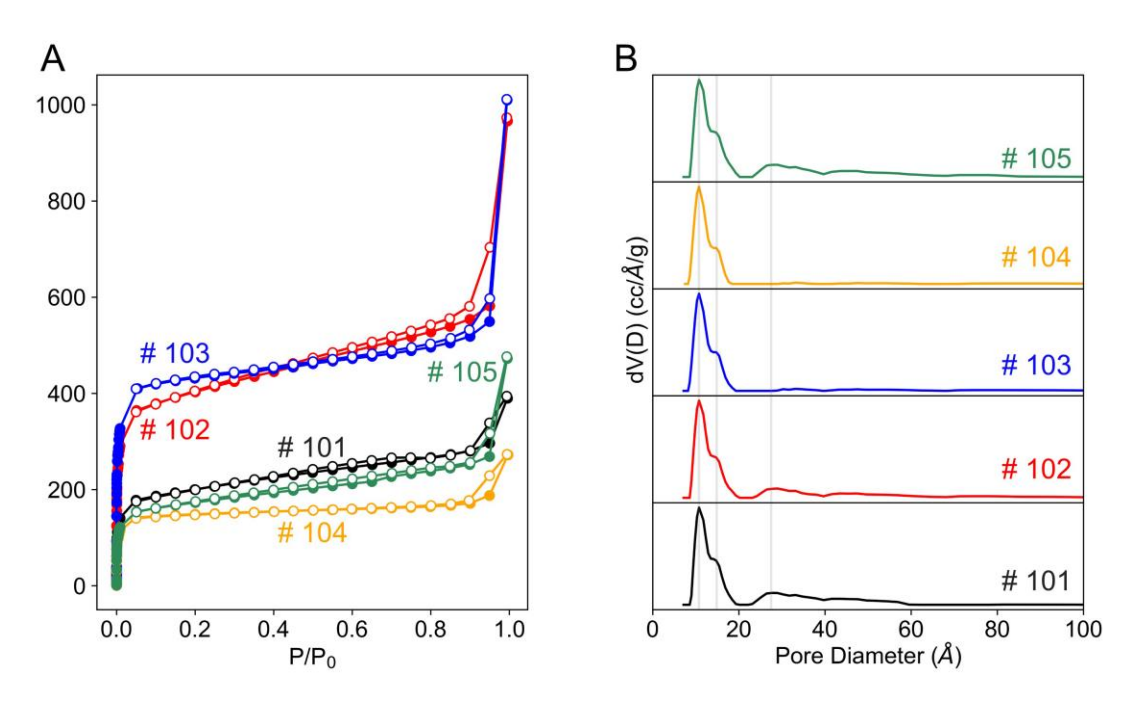


Figure S8. (A) Nitrogen sorption isotherms (77 K) and (B) pore size distributions of samples #101 to #105.

S6. CORRELATIONS OF TEXTURAL PROPERTIES OF THE SUCCESSFULLY SYNTHESIZED ZIF-8

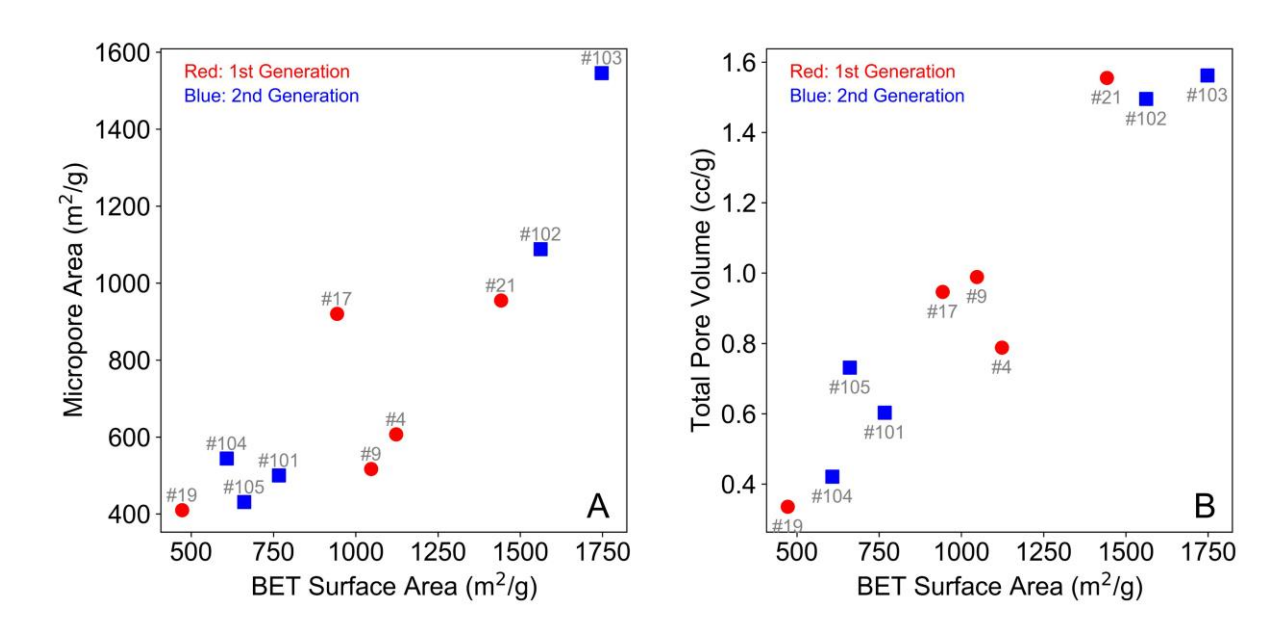


Figure S9. (A) Plot of BET surface areas vs micropore areas of the successfully synthesized ZIF-8; (B) Plot of BET surface areas vs total pore volumes of the successfully synthesized ZIF-8.

S7. SYNTHESIS OF ZIF-67 USING THE OPTIMIZED PARAMETERS FOR THE FORMATION OF ZIF-8 CRYSTALS

The synthesis parameters for the optimized ZIF-8 sample #103 were then applied for the synthesis of ZIF-67, which is isostructural to ZIF-8 but with Co²⁺ as the metal instead of Zn²⁺. The corresponding SEM images of the as-prepared ZIF-67 were shown below in **Figure S10**.

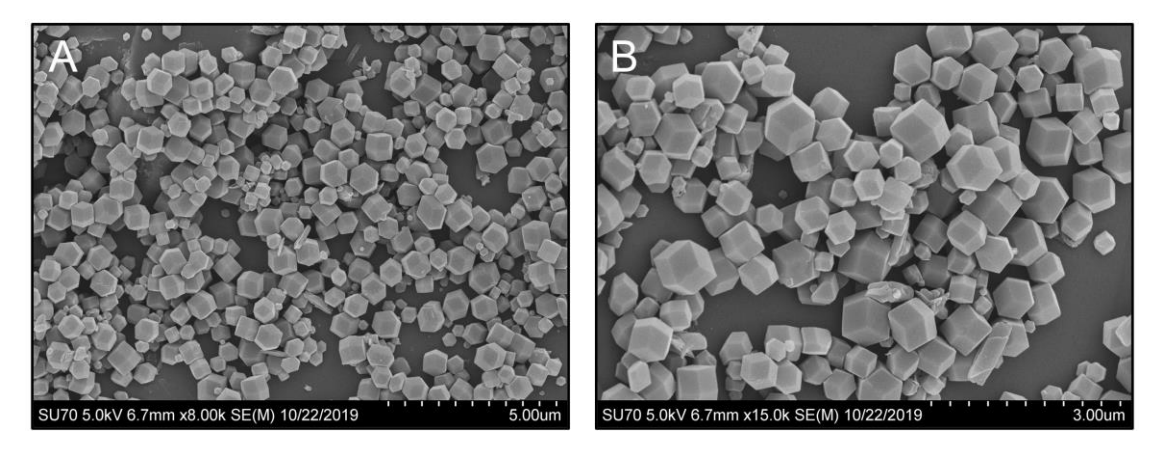


Figure S10. SEM images of as-prepared ZIF-67. Magnifications: (A) ×8k; (B) ×15k.

S8. REFERENCES

- 1. Collison Nebulizer, http://chtechusa.com/products_tag_lg_collison-nebulizer.php, (accessed 1 July 2020).
- 2. S. M. Moosavi, A. Chidambaram, L. Talirz, M. Haranczyk, K. C. Stylianou and B. Smit, *Nat. Commun.*, 2019, **10**, 539.